# Effect of TID Electron Radiation on SiGe BiCMOS LNAs at V-band

Flavien Sagouo Minko*, Tinus Stander

Carl & Emily Fuchs Institute for Microelectronics, Department of Electrical, Electronic & Computer Engineering, University of Pretoria, Pretoria 0002, SOUTH AFRICA

A R T I C LE I N FO

Keywords:
Total ionizing dose, Millimetre-wave circuits, Silicon germanium, SiGe HBT, low-noise amplifier

ABSTRACT

We investigate the effect of TID electron irradiation on a 65 GHz LNA in 130 nm SiGe BiCMOS. The LNA is exposed to a Sr-90 radiation source and irradiated at a rate of 200 krad (Si)/hr to a total dose of 15 Mrad(Si), with S-parameter and NF measurements taken at regular intervals. It is found that TID produces and increase in the input impedance, especially in the reactive component. The damage results in 2.3 dB reduction in midband gain, 2.97 dB increase in midband *NF* and up to 8.19 dB increase in midband $S_{11}$, although the device remains matched across the band of interest. The degradation is found most pronounced at the band-edges, yielding a 1 dB gain flatness bandwidth reduction of 32 %.

## 1. Introduction

Mm-wave bands are becoming increasingly important for applications in environments with ionizing radiation [1]. Such applications include 60 GHz inter-satellite communication [2] and radiometers [3], [4] as well as high bandwidth communication in high energy particle experiments [5]. V-band (50-75 GHz) front-end components, which are required for these applications, need to have some ionizing radiation tolerance. SiGe BiCMOS has proven to be a viable technology for mm-wave applications, with the 130 nm technology node (such as Globalfoundries US (formerly IBM) 8HP process [6]) enjoying widespread use. In addition, extensive irradiation testing (gamma, neutron and proton) have been conducted on SiGe devices, and have been found to cause only minor atomic displacement and ionization damage [7]–[9]. Other studies have also reported $r_b$ and $f_{Max}$ degradation after neutron irradiation [8], as an increase in $r_b$ results in a decrease in $f_{Max}$ based in (1). This has, however, been significantly reduced in 3rd generation SiGe[10], and is also not a primary consideration in reduced forward gain.

$$f_{max} = \sqrt{\frac{f_T}{8\times\pi\, r_b C_{jc}}} \tag{1}$$

A few studies have reported TID effects on SiGe HBT low noise amplifiers at different frequencies. In [11], a bias tuning method is adopted to mitigate the effect of 63.3 MeV proton irradiation on $|S_{21}|$

* Corresponding author
*E-mail address*: sagouominkof@tuks.co.za (F. Sagouo Minko)

and noise figure (*NF*) in a 10 GHz LNA. According to [12], the increased noise figure in the reported 60 GHz LNA is due to increased $r_b$, while the increase in the output reflection was associated to proton effect on microstrip transmission lines following 63.3-MeV proton exposure. The data in [13] indicates up to 94 % reduction in $|S_{21}|$, following electron irradiation at S-band. It is important to note that V-band LNAs in 3rd generation 130 nm BiCMOS are not included in these studies. These areas are particularly susceptible to trapped charges, which may alter the performance of an LNA [9].

This study presents the first mm-wave experimental data for electron radiation-induced degradation of LNAs in 3rd generation 130nm SiGe BiCMOS. The process and circuit under test are presented in Section II, and the test methodology in Section III. Section IV presents the consolidated results, with conclusions drawn in Section V.

## 2. The device under test (DUT)

The device under test is a two-stage low-noise amplifier, designed by the procedure outlined in [14] and first reported on in [15]. The circuit is fabricated in the GFUS 8HP 130nm SiGe BiCMOS process, which has been extensively studied in the literature for mm-wave circuitry [16] and TID tolerance [17], [18]. The process front-end-of-line (FEOL) cross-section for an HBT is depicted in Fig.1, as adapted from[19], [20]. Each of the two cascaded cascode stages uses two 0.12 × 4.5 µm HBTs, selected as a trade-off between gain and noise figure. Each branch is biased with constant base current sources, which force a collector current $I_C$ of 4.27 mA. Since the application required packaging of the LNA, the 100×100 µm bond pads were included in the circuit model, with pad parasitic capacitors compensated for by shunt stubs of +j29 Ω reactance value placed 26 µm from the signal pads and terminated in a 17 fF capacitor to increase its bandwidth. The circuit includes base and emitter degenerations for matching purposes (Fig. 3), as proposed in[21], [22], yielding the input impedance in (2) and (3). The required base degeneration was obtained by setting the real part of $Z_{in}$ in (3) equal to $Z_0$, while for emitter degeneration, the imaginary part of $Z_{in}$ was equated to zero. From (2) it is evident that the imaginary part of the input impedance is dominated by the base-emitter capacitance $C_{be}$ or $C_\pi$ at midband.

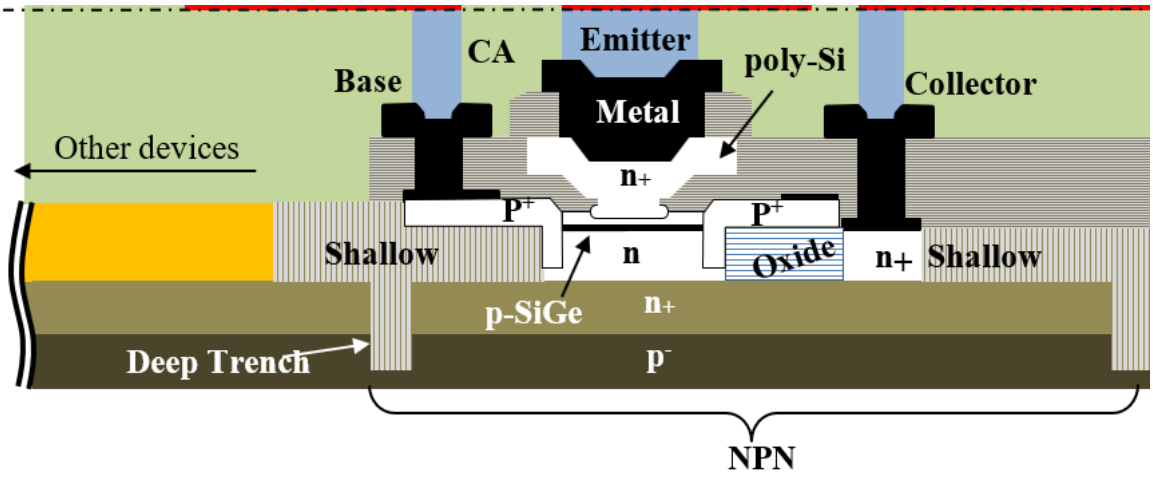


Fig. 1. Section of the front-end-of-line in BiCMOS8HP. Adapted from [19], [20]

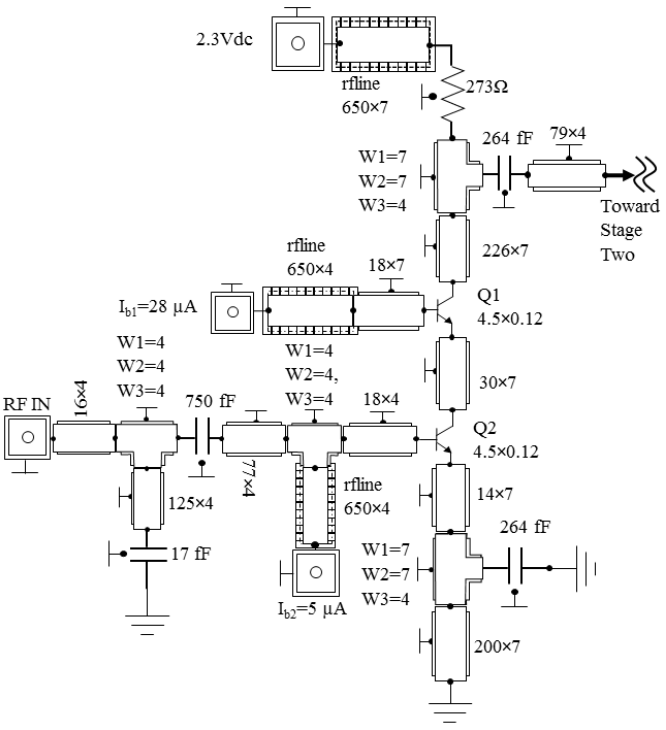


Fig. 2. The first stage of the V-band LNA schematic diagram using *pcell* components

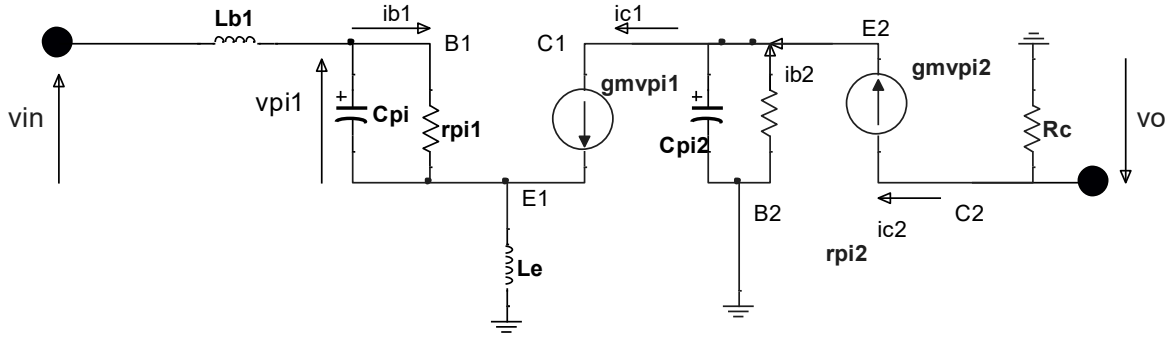


Fig. 3. Small signal model of the LNA including the base (Lb1) and emitter (Le) degeneration

$$Z_{in} = \frac{-j}{\omega C_{\pi 1}} + j\omega L_{e1} + \frac{g_{m1} L_{e1}}{C_{\pi 1}} + j\omega L_{b1} \tag{2}$$

$$Z_{in} = \frac{g_{m1} L_{e1}}{C_{\pi 1}} - j\left(\frac{1}{\omega C_{\pi 1}} - \omega L_{e1} - \omega L_{b1}\right) \tag{3}$$

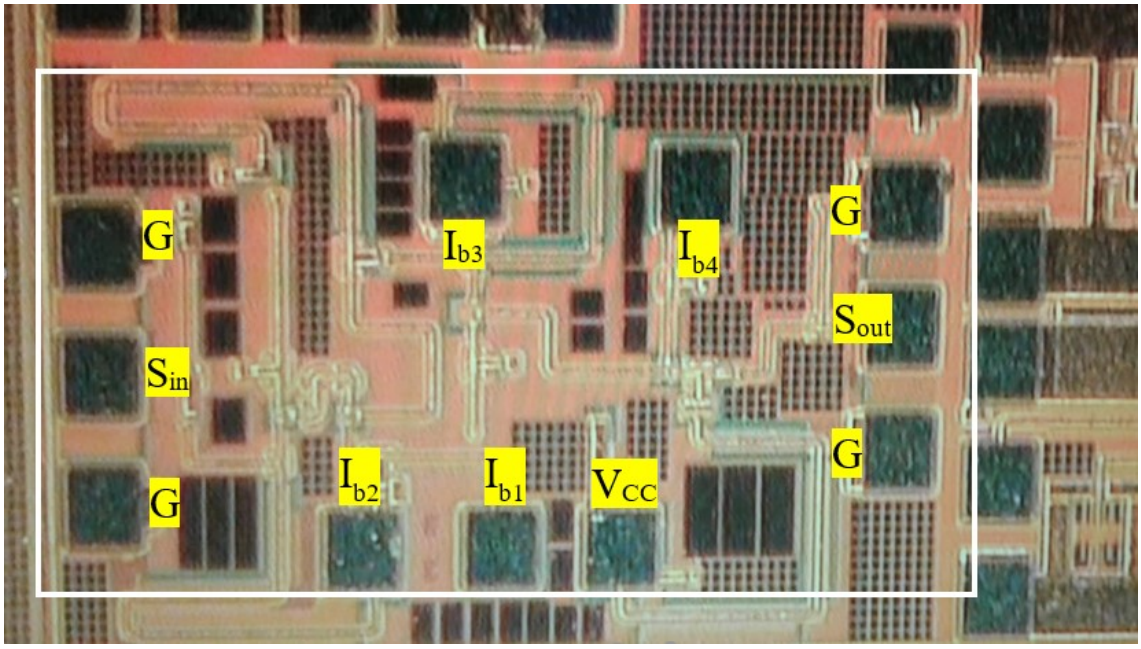


Fig. 4. Multi-project wafer highlighting the LNA

## 3. Test Methodology

### *3.1. RF characterization*

The LNA's linear S-parameters and NF were determined by wafer probing removed from the radiation source, as shown in Fig. 5. An HP4155B parameter analyzer was used to supply constant base currents, which forced the required dc collector current in each branch. For linear measurements, an Anritsu ME7828A VNA was used, with Line-Reflect-Match (LRM) first-tier calibration to move the calibration plane up to the GSG probe tips. Second-tier calibration (to remove pad parasitics) was not conducted, as the pad characteristics were included in the DUT design as required by the application.

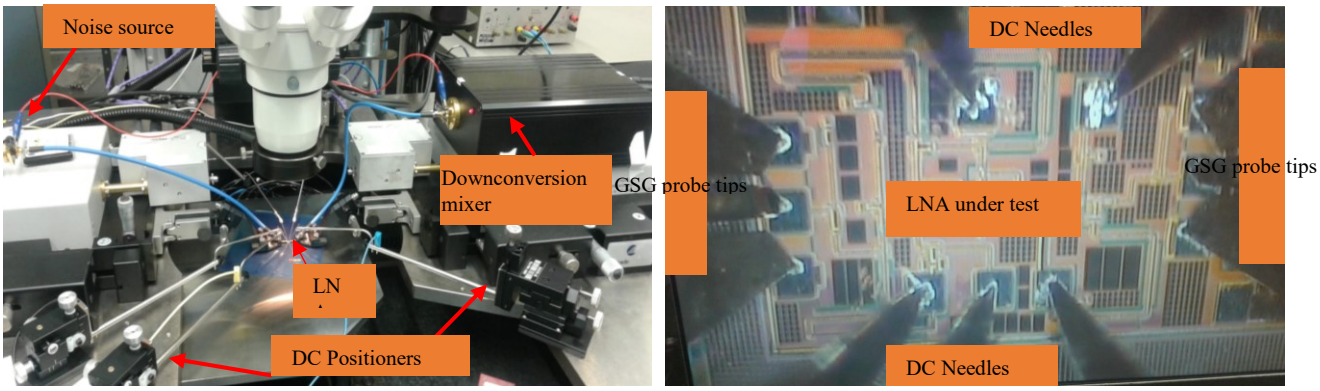


(a) (b)

Fig. 5. LNA under both noise figure (a) and S-parameter measurement (b)

For the noise figure measurement, the setup in Fig. 5a was used. The Rohde & Schwartz FSW50 signal and spectrum analyzer were used with the K-30 *NF* measurement option. The FSW was used with a Sage Millimeter low-noise block downconverter (STC-15-S1) and calibrated using a THRU standard on the impedance standards substrate used for VNA calibration. The noise integration bandwidth was set to 3 MHz. In addition to evaluating S-parameters and *NF*, degradation of the figure-

of-merit (*FoM*) was recorded, and calculated as:

$$FoM = \frac{G_{T(max)}B}{(F-1)P_{DC}} \quad (4)$$

where $G_T(max)$ is the maximum (matched) transducer gain in dB, $F$ is the noise factor at $f_0$, $P_{DC}$ the dc power consumed by the LNA in mW and $B$ the 1 dB gain flatness bandwidth. Before TID exposure, the measured midband $Z_{in}$ was 43+j5 Ω, translating to $|S_{11}|$ of -22 dB. The midband forward transmission $|S_{21}|_{max}$ was 14.8 dB, and the midband $NF$ =6.64 dB, resulting in an $FoM$ = 1.98.

### *3.2.Electron irradiation*

The radiation experiment was conducted remotely at a secure radiation facility under zero bias. Samples were irradiated with a Strontium Sr-90 electron radiation source of 3.4 GBq radioactivity [23]. The source releases an electron with a peak energy of ≈0.548 MeV (average 210 keV) during the first decay yielding Yttrium-90 and ≈2.26 MeV (average 890 keV), yielding Zirconium-90 [24] during the second decay.

The radiation source was placed at a height of 0.4 cm above the DUT, resulting in an approximate dose rate of 200 krad(Si)/hr [23]. The dose rate was verified using GafChromic EBT3 film (Fig 6b), with a measured uniformity within 10% over the die area. The sample was placed on a test bench as indicated in Fig. 6a, and was shielded with lead bricks. The accumulated doses are tabulated in Table 1, with five cumulative radiation doses considered over a period of 75 hrs. In all cases, samples were removed from radiation, electrically characterized, and returned to radiation within 1 hr.

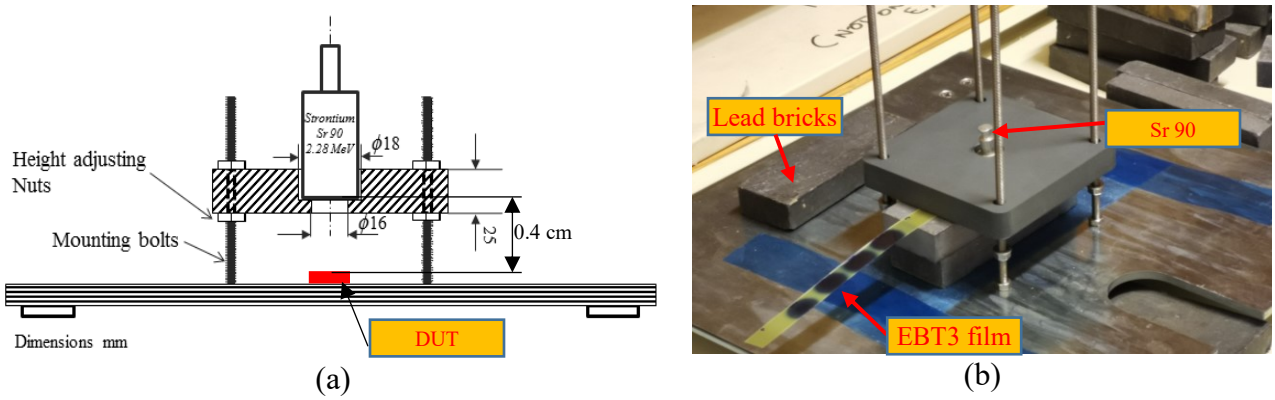


Fig. 6. Radiation experiment, a) Radiation platform configuration, b) measurement of the dose rate

## 4. Results and discussion

The results of the experiment are tabulated in Table 1. We observe a gradual reduction of both $|S_{21}|$ and bandwidth, with an increase in $NF$ and $I_C$, all culminating in a reduction in $FoM$. The frequency responses for $|S_{21}|$ and $NF$ are shown in Figs. 7 and 11, respectively. Although these changes may be modelled explicitly, in simulation, using the methods described in [25], the published method is not scalable with biasing or device size (nor do any models exist with which this is possible). Implementing exact simulation models, as are derived in [25], would therefore require small-signal pre-characterization of the amplifier's constituent transistors, in isolation, under identical bias conditions. As these transistors were not available, the simulation model cannot be adapted to a specific dose. We may, however, infer trends from [25], and apply it to our discussion on the measurement results we observed.

Of particular interest is the reduction in 1 dB gain flatness bandwidth in addition to the reduction in mid-band gain. The increased lower cut-off may be attributed to damaged metal insulation metal (MIM) capacitors (the values of which would decrease over increased dose [26]) used as coupling and bypass capacitors, while the decreased upper cut-off may be attributed to increases in the intrinsic parameters $R_{be}$ ($R_b$+$R_e$) and $C_{be}$ [25]. The combination of these effects would result in the reduced pass-band bandwidth, as indicated in Fig. 2 [27].

The increase in return loss, shown in Fig. 8 and 9, would further indicate changes in the base-emitter capacitance $C_\pi$ and resistance $r_\pi$ (considering the π-model), which would ultimately impact both $|S_{21}|$ and *NF* as well. This view is substantiated by Fig. 10, which would indicate an increase in input capacitance and resistance midband with increasing dose. Both of these observations are in line with the data reported in[10], [25] and [28], where electron radiation TID damage is associated with increased $R_{be}$ and $C_{be}$. Charge trapped in the shallow and deep trench isolations below the distributed inductors labelled *rfline* in Fig. 2 would also increase sidewall capacitor due to changes in the oxide dielectric (see Fig. 1), further increasing the observed input capacitance.

The reduction in |S21| can be attributed to the reduction in small-signal transconductance, as reported in [25]. The increase in NF may be attributed to the same phenomenon, as well as the increase of base thermal noise due to increased $R_{bi}$ [29], which is also documented in [25]. This view is also supported by Fig. 10, which shows an increase in input resistance, in in line with what is reported in [28]. The increases $I_{CQ}$ may also contribute to increased collector shot noise, further increasing NF [29]. Both reduced gain and increased *NF* are further supported by previous experiments [28], [30].

Finally, the recorded increase in collector current, despite constant base bias current, may be attributed to various effects. It may be attributed to increased effective base current as a result of trapped charges between the emitter-base junction [8] [13]. The sudden increase (as observed in Fig 12) under moderate damage, however, is contrary to the gradual degradation observed in other performance parameters. This might indicate a leakage path created by a radiation-induced defect, possibly in one of the large 264 fF MIM capacitors in Fig 2 used for RF grounding [25]. Another possibility is increased collector current density, which increases with TID but plateaus at values above ≈ 1 MRad for the TID gamma irradiation in [29].

Table 2 presents a comparison of this study with other TID studies on SiGe LNAs in the literature. The data would indicate very limited open sources data in electron radiation effect on mm-wave LNAs. In [13], where electron irradiation is investigated, *NF* degradation data is not provided, nor is the FoM. It is, however, interesting to note the severe gain degradation observed under electron radiation > 10 Mrad(Si), both in this work and in [13], while SiGe's resilience to irradiation in [19] is only discussed in terms of gamma, neutron and proton radiation.

Table 1: TID radiation degradation results

| **Parameters** | **Pre-Rad** | **1.5 Mrad** | **3.75 Mrad** | **7.5 Mrad** | **11.25 Mrad** | **15 Mrad** |
|---|---|---|---|---|---|---|
| $P_{DC}$(mW) | 9.89 | 15.87 | 14.26 | 14.28 | 14.26 | 14.3 |
| FoM | 1.98 | 0.9 | 0.87 | 0.66 | 0.47 | 0.35 |
| $Z_{in}$ (Ω) | 43+j5 | 43.5+j3.5 | 43.56+j2 | 43.7+j0.35 | 44+j0.002 | 44-j9.45 |
| $\|S_{21}\|_{(max)}$ (dB) | 14.8 | 13.93 | 13 | 12.62 | 12.4 | 12.3 |
| NF (dB) | 6.64 | 7.2 | 7.42 | 8.2 | 9.1 | 9.5 |
| BW (GHz) | 4.8 | 4.45 | 4.24 | 4.2 | 3.85 | 3.25 |

Table 2: Proton and electron irradiation effects on SiGe LNAs.

| **Reference** | [13] | [12] | [11] | **This work** |
|---|---|---|---|---|
| Radiation type | Electron, 3 MeV | Proton, 63.3 MeV | Proton, 63.3 MeV | Electron, 2.26 MeV |
| $f_0$ (GHz) | 2.5 | 62 | 12 | 65 |
| Total dose (Mrad(si)) | 25 | 0.134 | 2 | 15 |
| Pre-rad $\|S_{21}\|_{(max)}$ (dB) | 20.9 | 14.2 | 17.5 | 15 |
| Post-rad $\|S_{21}\|_{(max)}$ (dB) | 7.5 | 13.6 | 17.3 | 13.7 |
| Pre-rad NF (dB) | - | 3 | 5.85 | 6.5 |
| Post-rad NF (dB) | - | 3.5 | 5.63 | 7.72 |
| Pre-rad $I_C$ (mA) | - | 8 | 3.5 | 4.5 |
| Post-rad $I_C$ (mA) | - | 8 | 3.5 | 6.9 |

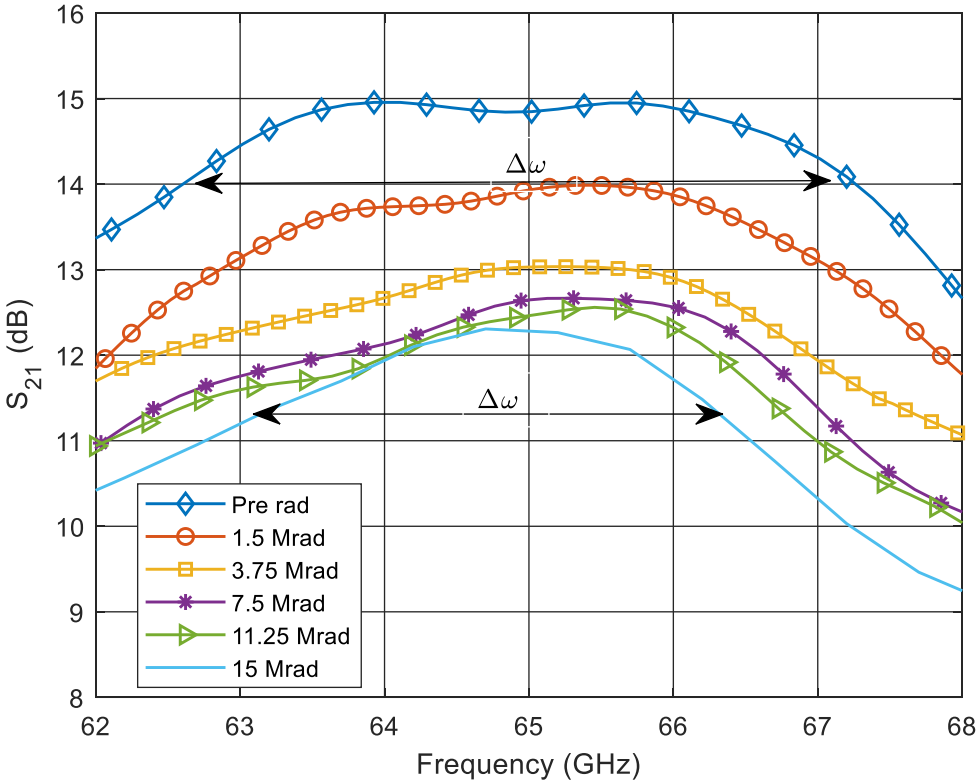


Fig. 7. LNA gain pre- and post-radiation following each incremental radiation dose

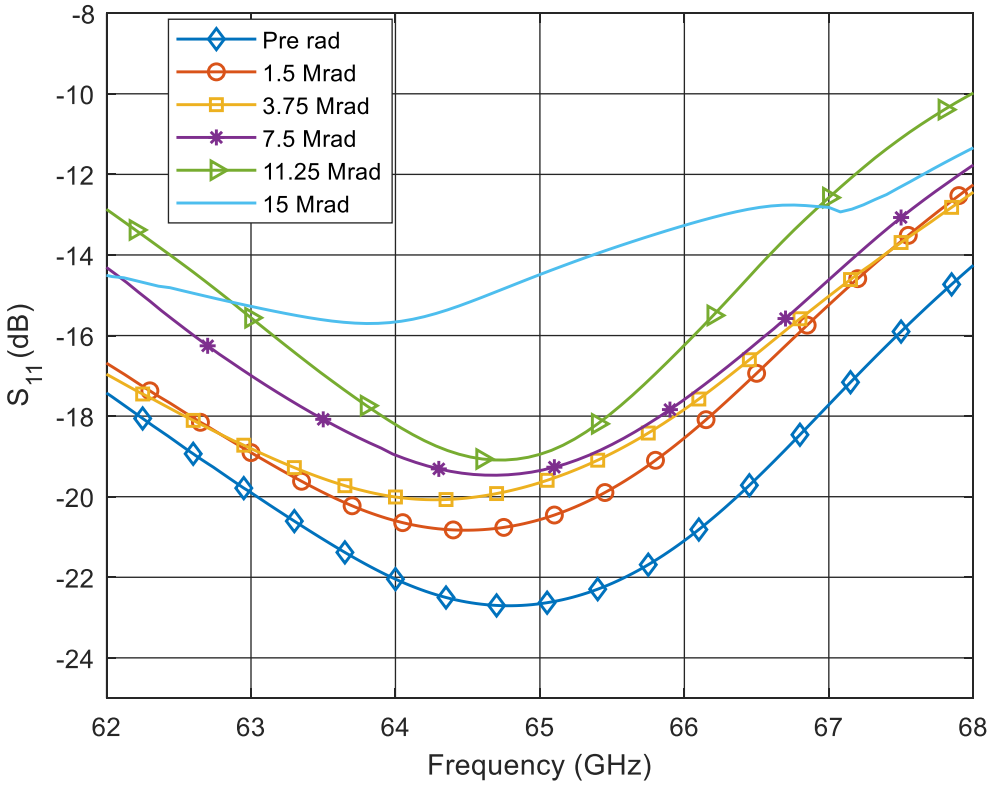


Fig. 8. LNA input match pre- and post-radiation on a rectangular plot

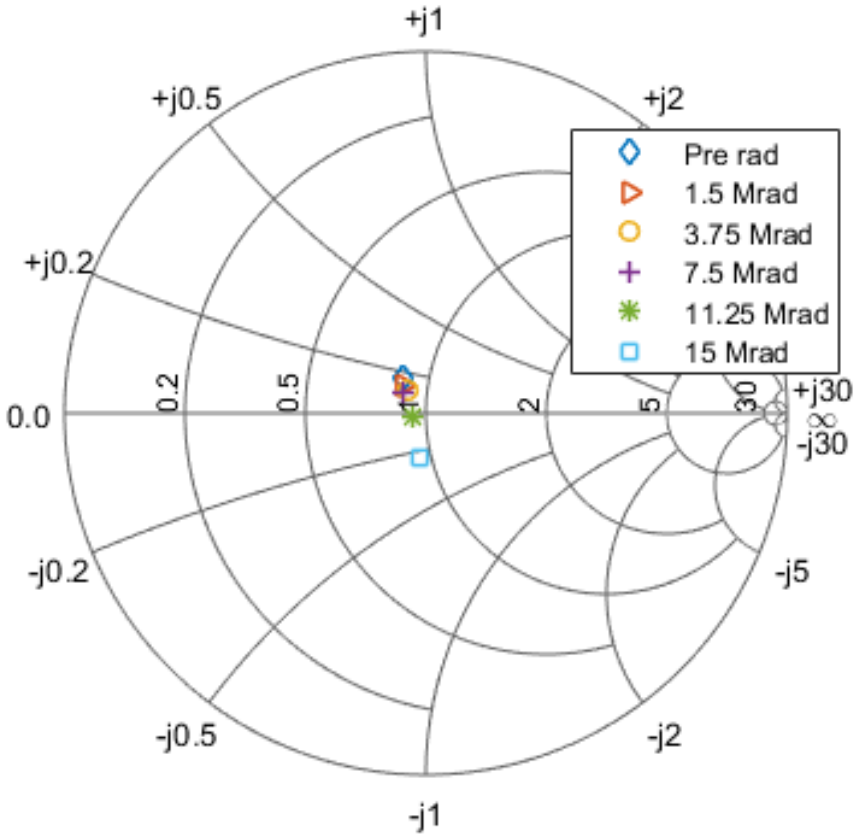


Fig. 10. LNA input impedance pre- and post-radiation on a Smith chart

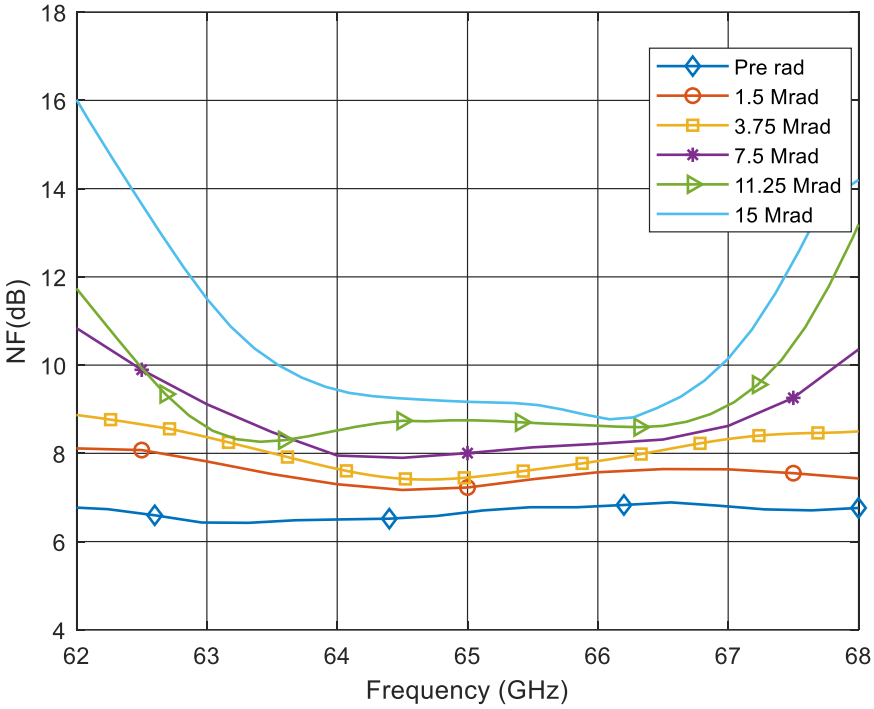


Fig. 11. LNA noise figure pre- and post-radiation for each dose

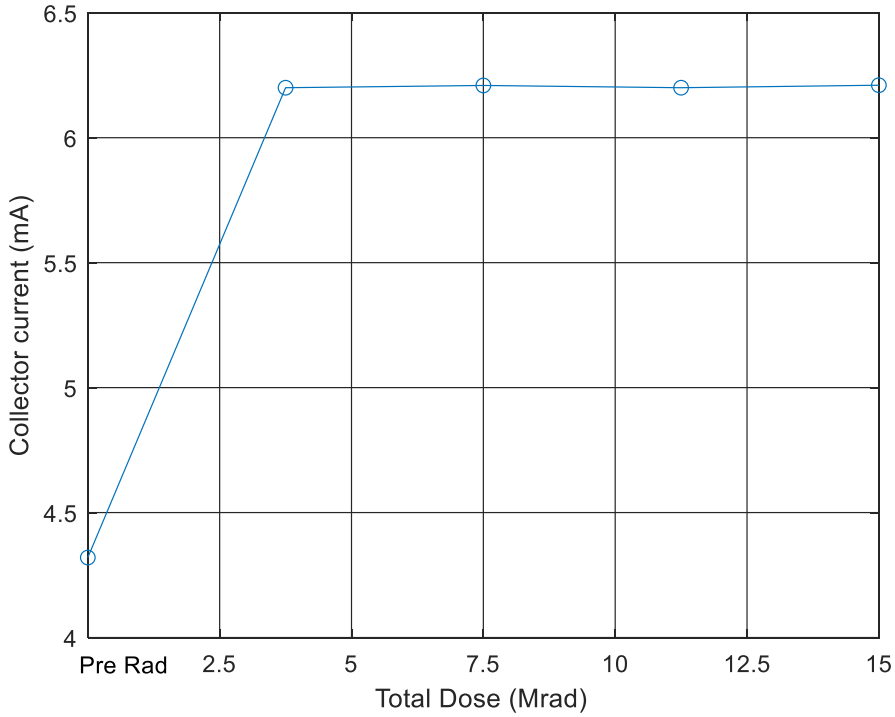


Fig. 12. $I_C$ vs. radiation dose

## 5. Conclusion

The susceptibility of mm-wave circuitry in 130nm SiGe BiCMOS to electron radiation damage has been evaluated for the first time at V-band, by measuring the degradation of a 65 GHz SiGe HBT LNA under electron exposure from a Sr-90 source. Approximately 3 dB reduction in the forward gain and *NF* were observed up to a total dose of 15 Mrad(Si), along with significantly reduced bandwidth of 1

dB gain flatness and minor increase of return loss. The results are in line with prior reported results in other technologies and other frequencies.

## Acknowledgement

The authors wish to thank the MOSIS Educational Programme (MEP) for the support given in sponsoring the prototyping space in the GFUS 8HP process, as well as the Department of Physics at the University of Pretoria for availing their radiation test facility for the duration of the experiment. This work was sponsored by the National Research Foundation of South Africa (NRF) under grants UID 92526 and 93921.

## References

[1] F. Alimenti, V. Palazzari, A. Battistini, L. Aluigi, S. M. WHITE, and L. ROSELLI, 'A System-on-Chip millimeter-wave radiometer for the space-based observation of solar flares', in *15th Conference on Microwave Techniques COMITE 2010*, Apr. 2010, pp. 3–8, doi: 10.1109/COMITE.2010.5481710.

[2] Chinmayi A V, M. S. Vasanthi, and T. R. Rao, 'Performance evaluation of RF based Inter Satellite communication Link at 60 GHz', in *2016 International Conference on Wireless Communications, Signal Processing and Networking (WiSPNET)*, Mar. 2016, pp. 59–64, doi: 10.1109/WiSPNET.2016.7566090.

[3] S. C. Reising *et al.*, 'Microwave and millimeter-wave radiometers for CubeSat deployment for remote sensing of the earth's atmosphere', in *2014 39th International Conference on Infrared, Millimeter, and Terahertz waves (IRMMW-THz)*, Sep. 2014, pp. 1–1, doi: 10.1109/IRMMW-THz.2014.6956214.

[4] W. Williams, C. Coen, M. Frounchi, N. Lourenco, and J. D. Cressler, 'Micronimbus: A cubesat temperature profilometer for the earth's atmosphere using a single-chip 60 GHZ sige radiometer', in *2017 IEEE International Geoscience and Remote Sensing Symposium (IGARSS)*, Jul. 2017, vol. 7, pp. 2740–2743, doi: 10.1109/IGARSS.2017.8127564.

[5] S. Dittmeier, A. Schöning, H. K. Soltveit, and D. Wiedner, 'Feasibility studies for a wireless 60 GHz tracking detector readout', *Nucl. Instrum. Methods Phys. Res. Sect. Accel. Spectrometers Detect. Assoc. Equip.*, vol. 830, pp. 417–426, 2016, doi: 10.1016/j.nima.2016.06.016.

[6] J. S. Dunn *et al.*, 'Foundation of rf CMOS and SiGe BiCMOS technologies', *IBM J. Res. Dev.*, vol. 47, no. 2.3, pp. 101–138, Mar. 2003, doi: 10.1147/rd.472.0101.

[7] S. Diez *et al.*, 'Proton Radiation Damage on SiGe:C HBTs and Additivity of Ionization and Displacement Effects', *IEEE Trans. Nucl. Sci.*, vol. 56, no. 4, pp. 1931–1936, Aug. 2009, doi: 10.1109/TNS.2009.2018552.

[8] J. M. Roldan, W. E. Ansley, J. D. Cressler, S. D. Clark, and D. Nguyen-Ngoc, 'Neutron radiation tolerance of advanced UHV/CVD SiGe HBT BiCMOS technology', *IEEE Trans. Nucl. Sci.*, vol. 44, no. 6, pp. 1965–1973, Dec. 1997, doi: 10.1109/23.658970.

[9] A. K. Sutton *et al.*, 'A comparison of gamma and proton radiation effects in 200 GHz SiGe HBTs', *IEEE Trans. Nucl. Sci.*, vol. 52, no. 6, pp. 2358–2365, Dec. 2005, doi: 10.1109/TNS.2005.860728.

[10] Yuan Lu *et al.*, 'Proton tolerance of third-generation, 0.12 /spl mu/m 185 GHz SiGe HBTs', *IEEE Trans. Nucl. Sci.*, vol. 50, no. 6, pp. 1811–1815, Dec. 2003, doi: 10.1109/TNS.2003.820737.

[11] D. C. Howard *et al.*, 'An 8–16 GHz SiGe Low Noise Amplifier With Performance Tuning Capability for Mitigation of Radiation-Induced Performance Loss', *IEEE Trans. Nucl. Sci.*, vol. 59, no. 6, pp. 2837–2846, Dec. 2012, doi: 10.1109/TNS.2012.2224132.

[12] W.-M. L. Kuo, B. M. Haugerud, W. Marshall, R. A. Reed, and G. Freeman, 'Total Dose Tolerance of Monolithic Millimeter-Wave Transceiver Building Blocks Implemented in 200 GHz SiGe Technology', p. 7.

[13] A. S. Youssouf, M. H. Habaebi, S. N. Ibrahim, and N. F. Hasbullah, 'Gain Investigation for commercial GaAs and SiGe HBT LNA's under Electron irradiation', in *2016 IEEE Student Conference on Research and Development (SCOReD)*, Dec. 2016, pp. 1–5, doi: 10.1109/SCORED.2016.7810094.
[14] A. Y. K. Chen, Y. Baeyens, Y. K. Chen, and J. Lin, 'A Low-Power Linear SiGe BiCMOS Low-Noise Amplifier for Millimeter-Wave Active Imaging', *IEEE Microw. Wirel. Compon. Lett.*, vol. 20, no. 2, pp. 103–105, Feb. 2010, doi: 10.1109/LMWC.2009.2038528.
[15] F. S. Minko and T. Stander, 'A comparison of three-dimensional electromagnetic and RC parasitic extraction analysis of mm-wave on-chip passives in SiGe BiCMOS low-noise amplifiers', *Int. J. RF Microw. Comput.-Aided Eng.*, vol. 30, no. 2, p. e22019, 2020, doi: 10.1002/mmce.22019.
[16] B. A. Floyd, S. K. Reynolds, U. R. Pfeiffer, T. Zwick, T. Beukema, and B. Gaucher, 'SiGe bipolar transceiver circuits operating at 60 GHz', *IEEE J. Solid-State Circuits*, vol. 40, no. 1, pp. 156–167, Jan. 2005, doi: 10.1109/JSSC.2004.837250.
[17] J. S. Rice *et al.*, 'Performance of the SiGe HBT 8HP and 8WL Technologies after High Dose/Fluence Radiation Exposure', in *2008 IEEE Nuclear Science Symposium Conference Record*, Oct. 2008, pp. 2206–2210, doi: 10.1109/NSSMIC.2008.4774790.
[18] J. Metcalfe *et al.*, 'Evaluation of the radiation tolerance of several generations of SiGe heterojunction bipolar transistors under radiation exposure', *Nucl. Instrum. Methods Phys. Res. Sect. Accel. Spectrometers Detect. Assoc. Equip.*, vol. 579, no. 2, pp. 833–838, Sep. 2007, doi: 10.1016/j.nima.2007.05.328.
[19] H. Rucker and B. Heinemann, 'SiGe BiCMOS technology for mm-wave systems', in *SoC Design Conference (ISOCC), 2012 International*, Nov. 2012, pp. 266–268, doi: 10.1109/ISOCC.2012.6407091.
[20] J. D. Cressler, 'Radiation Effects in SiGe Technology', *IEEE Trans. Nucl. Sci.*, vol. 60, no. 3, pp. 1992–2014, Jun. 2013, doi: 10.1109/TNS.2013.2248167.
[21] W.-L. Kuo, Qingqing Liang, J. D. Cressler, and M. A. Mitchell, 'An X-band SiGe LNA with 1.36 dB mean noise figure for monolithic phased array transmit/receive radar modules', in *IEEE Radio Frequency Integrated Circuits (RFIC) Symposium, 2006*, Jun. 2006, pp. 4 pp. – 501, doi: 10.1109/RFIC.2006.1651200.
[22] T. K. Thrivikraman *et al.*, 'A 2 mW, Sub-2 dB Noise Figure, SiGe Low-Noise Amplifier For X-band High-Altitude or Space-based Radar Applications', in *2007 IEEE Radio Frequency Integrated Circuits (RFIC) Symposium*, Jun. 2007, pp. 629–632, doi: 10.1109/RFIC.2007.380962.
[23] B. Habeenzu, W. Meyer, and T. Stander, 'Effect of electron radiation on small-signal parameters of NMOS devices at mm-wave frequencies', *Microelectron. Reliab.*, vol. 107, p. 113598, Apr. 2020, doi: 10.1016/j.microrel.2020.113598.
[24] B. Pajic and R. H. Greiner, 'Long term results of non-surgical, exclusive strontium-/yttrium-90 beta-irradiation of pterygia', *Radiother. Oncol.*, vol. 74, no. 1, pp. 25–29, Jan. 2005, doi: 10.1016/j.radonc.2004.08.022.
[25] B. Habeenzu, 'TID induced small signal model variation in CMOS and SiGe BiCMOS', University of Pretoria, Pretoria, 2019.
[26] B. Miao, R. Mahapatra, R. Jenkins, J. Silvie, N. G. Wright, and A. B. Horsfall, 'Radiation Induced Change in Defect Density in HfO-Based MIM Capacitor', *IEEE Trans. Nucl. Sci.*, vol. 56, no. 5, pp. 2916–2924, Oct. 2009, doi: 10.1109/TNS.2009.2015314.
[27] D. A. Neamen, *Microelectronics Circuit Analysis and Design*. McGraw-Hill Education, 2009.
[28] Shiming Zhang, Guofu Niu, J. D. Cressler, S. D. Clark, and D. C. Ahlgren, 'The effects of proton irradiation on the RF performance of SiGe HBTs', *IEEE Trans. Nucl. Sci.*, vol. 46, no. 6, pp. 1716–1721, Dec. 1999, doi: 10.1109/23.819144.
[29] J. C. Bardin, 'Silicon-Germanium Heterojunction Bipolar Transistors for Extremely Low-Noise Applications', phd, California Institute of Technology, 2009.

[30] J. A. Babcock, J. D. Cressler, L. S. Vempati, S. D. Clark, R. C. Jaeger, and D. L. Harame, ‘Ionizing radiation tolerance of high-performance SiGe HBT’s grown by UHV/CVD’, *IEEE Trans. Nucl. Sci.*, vol. 42, no. 6, pp. 1558–1566, Dec. 1995, doi: 10.1109/23.488750.